

ARTICLE OPEN

Unveiling the hidden nematicity and spin subsystem in FeSe

Chih-Wei Luo^{1,2}, Po Chung Cheng¹, Shun-Hung Wang³, Jen-Che Chiang³, Jiunn-Yuan Lin³, Kaung-Hsiung Wu¹, Jenh-Yih Juang¹, Dmitry A. Chareev^{4,5,6}, Olga S. Volkova^{5,7,8} and Alexander N. Vasiliev^{7,8,9}

The nematic order (nematicity) is considered as one of the essential ingredients to understand the mechanism of Fe-based superconductivity. In most Fe-based superconductors (pnictides), nematic order is reasonably close to the antiferromagnetic order. In FeSe, in contrast, a nematic order emerges below the structure phase transition at $T_s = 90$ K with no magnetic order. The case of FeSe is of paramount importance to a universal picture of Fe-based superconductors. The polarized ultrafast spectroscopy provides a tool to probe simultaneously the electronic structure and the magnetic interactions through quasiparticle dynamics. Here we show that this approach reveals both the electronic and magnetic nematicity below and, surprisingly, its fluctuations far above T_s to at least 200 K. The quantitative pump–probe data clearly identify a correlation between the topology of the Fermi surface and the magnetism in all temperature regimes, thus providing profound insight into the driving factors of nematicity in FeSe and the origin of its uniqueness.

npj Quantum Materials (2017)2:32; doi:10.1038/s41535-017-0036-5

INTRODUCTION

The progress in understanding Fe-based superconductors has formed a most intriguing chapter in modern condensed matter physics.^{1–3} The existence of nematic order has become well established in Fe-based superconductors and is considered an essential ingredient to understand the mechanism of Fe-based superconductivity.^{4–6} The nematic order breaks the rotational symmetry by making the x and y directions in the plane non-equivalent, while preserving the time-reversal symmetry. The chalcogenide FeSe has a superconducting transition temperature $T_c \sim 8.5$ K; its tetragonal structure undergoes a transition to orthorhombic below $T_s = 90$ K. No long-range magnetic order has ever been detected in FeSe down to the lowest temperatures.^{7–10} In this respect, as the structurally simplest Fe-based superconductor, FeSe has unexpectedly emerged in the frontier of Fe-based superconductivity research.^{11–25} Up to date, few consensus have been reached on either the electronic structure of FeSe or its nematic and superconducting mechanisms. For example, very recent angle-resolved photoemission spectroscopy (ARPES) has indicated a small Fermi surface (FS) above T_s that cannot be reproduced by density functional theory calculations.^{10, 14–16, 26–28} Furthermore, various ARPES groups concur on an even smaller FS below T_s ,^{10, 14–16, 26–30} which is in general consistent with the Sommerfeld coefficient observed from the specific heat.^{31, 32} Nevertheless, how and why a FS is reconstructed in FeSe through T_s is poorly characterized. As for the nematic order under T_s , almost everyone agrees on an electronic origin, as a 0.2% orthorhombic distortion is unlikely to lead to the observed FS elongation and the shift of band energy at the M point.¹⁵ Nevertheless, whether the nematicity in FeSe is magnetically or orbitally driven is under current fierce debate, whereas it is generally considered to be driven by magnetism in pnictides.⁶

This controversy occurs largely due to the absence of the magnetic order in FeSe that remains an unsolved puzzle. The existence of nematic fluctuations above T_s is, likewise, not entirely clear in the literature.

In the present work, we utilized the polarized femtosecond pump–probe spectroscopy of FeSe to elucidate the above issues. This probe is relevant to both the charge and spin channels, and is sensitive to fluctuations or the short-range order. For example, the wavelength-dependent femtosecond spectroscopy clearly revealed the magnetic fluctuations at $T = 170$ K in HoMnO_3 , far above the long-range antiferromagnetic $T_N = 76$ K.³³ A similar technique has been applied to detect the nematic fluctuations above T_s in pnictides.^{34–36} Here we employed polarized ultrafast spectroscopy to elucidate the detailed orientation and temperature dependence of the quasiparticle dynamics in FeSe. As a result of this comprehensive survey, the hidden nematic fluctuations and spin subsystem in FeSe are unveiled.

RESULTS

Figure 1 shows the typical polarization-dependent photoinduced reflectivity ($\Delta R/R$) transients on the (001) plane of an FeSe single crystal at various temperatures. At $T = 60$ K, below T_s , the $\Delta R/R$ transients demonstrate clear nematicity (Fig. 1a) in this phase, as also indicated in other experiments.^{10, 14–16, 26–28} We show below that this nematicity in dynamics reveals information of both the quasiparticle and magnetic channels. Astonishingly, $\Delta R/R$ shows profound nematic fluctuations even at $T = 150$ K, far above T_s (Fig. 1b); this two-fold symmetry persists up to at least 200 K (Fig. 2c). Overall, the raw data in Fig. 1 indicate clear nematic signals in ultrafast dynamics at the highest temperatures unprecedented in preceding reports. Furthermore, the two-fold

¹Department of Electrophysics, National Chiao Tung University, Hsinchu 300, Taiwan; ²Taiwan Consortium of Emergent Crystalline Materials, Ministry of Science and Technology, Taipei 10601, Taiwan; ³Institute of Physics, National Chiao Tung University, Hsinchu 300, Taiwan; ⁴Institute of Experimental Mineralogy, Russian Academy of Sciences, Chernogolovka, Moscow 142432, Russia; ⁵Institute of Physics and Technology, Ural Federal University, Mira street 19, Ekaterinburg 620002, Russia; ⁶Kazan Federal University, 18 Kremlyovskaya Str., Kazan 420008, Russia; ⁷Physics Faculty, Moscow State University, Moscow 119991, Russia; ⁸National University of Science and Technology “MISIS”, Moscow 119049, Russia and ⁹National Research South Ural State University, Chelyabinsk 454080, Russia
Correspondence: Chih-Wei Luo (cwluo@mail.nctu.edu.tw) or Jiunn-Yuan Lin (ago@cc.nctu.edu.tw)

Received: 15 September 2016 Revised: 16 May 2017 Accepted: 25 May 2017

Published online: 28 June 2017

symmetry pattern shifts by 90° when the temperature passes through T_s as shown in Fig. 1. To depict the context of Fig. 1 more clearly, Fig. 2 shows the typical $\Delta R/R$ transients with the electric

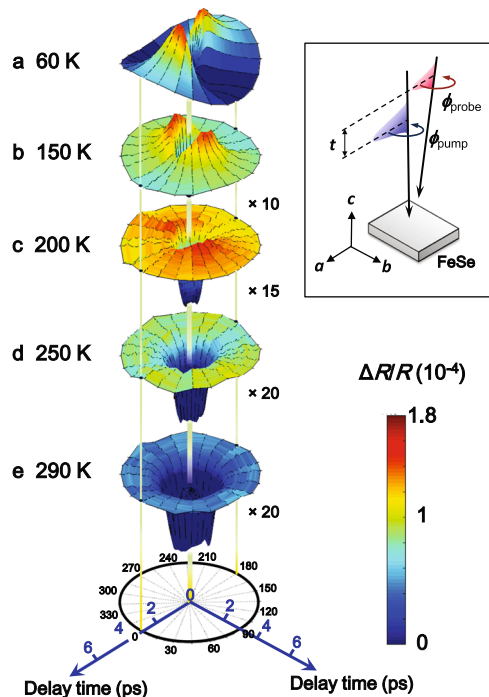


Fig. 1 Three-dimensional plot of orientation-dependent photoinduced reflectivity ($\Delta R/R$) transients at various temperatures. *Inset*: schematics of the experimental setup of polarization-dependent pump-probe spectroscopy. $\phi_{\text{pump}} = 0^\circ$ and $\phi_{\text{probe}} = 0^\circ$ indicate that the \mathbf{E} field of pump and probe pulses along a -axis of an FeSe single crystal

field \mathbf{E} along $\phi = 0^\circ$ and $\phi = 90^\circ$ at the temperatures associated with those in Fig. 1. (Angles $\phi = 0^\circ$ and $\phi = 90^\circ$ were chosen to represent the largest nematic signals, which are corresponding to a -axis and b -axis of orthorhombic structure, respectively.) Both the sign and the amplitude of $\Delta R/R$ transients show clear nematicity between $\phi = 0^\circ$ and $\phi = 90^\circ$ at 60 K, as shown in Fig. 2a. With T increasing to 150 K, the sign of $\Delta R/R$ transients along $\phi = 90^\circ$ markedly reverses from negative to positive. Although this pattern shift was unexpected, it manifests a valuable clue to the coupling between magnetism and the FS topology in FeSe, as discussed below.

The relaxation processes ($t > 0$) of $\Delta R/R$ transients in FeSe single crystals are described phenomenologically with

$$\frac{\Delta R}{R} = A_1 e^{-\frac{t}{\tau_1}} + A_2 e^{-\frac{t}{\tau_2}} + A_0 \quad (1)$$

The first term in the right side of Eq. 1 is the decay of the photoexcited electrons (or quasiparticles, QPs) with an initial population number A_1 , through phonon coupling with a relaxation time τ_1 . The second term pertains to the decay of QPs with an initial population number A_2 , through spin coupling with a corresponding decay time τ_2 . The third term describes the energy loss from the hot spot to the ambient environment on a time scale of microsecond, which is much longer than the period of the measurement (~ 50 ps) and is hence taken as a constant. The ascriptions of the first and the second terms are due mainly to the time and energy scales of τ_1 and τ_2 . (See the sections S2, S3 and S4 in Supplementary Information).

To depict better the temperature dependence of nematic ultrafast dynamics, we undertook another thorough run of $\Delta R/R$ transient measurements with \mathbf{E} along both $\phi = 0^\circ$ and $\phi = 90^\circ$. According to Eq. 1, each component was extracted from 290 to 30 K, as shown in Fig. 3a–d. We discuss first the results for $T \leq T_s$; this nematic phase of FeSe has been defined better than the state of $T > T_s$. For the fast component in $\Delta R/R$, a remarkable difference in the amplitude A_1 was observed between $\phi = 0^\circ$ and $\phi = 90^\circ$ in the low-temperature regime, shown in Fig. 3a. For $\phi = 0^\circ$, the sign of

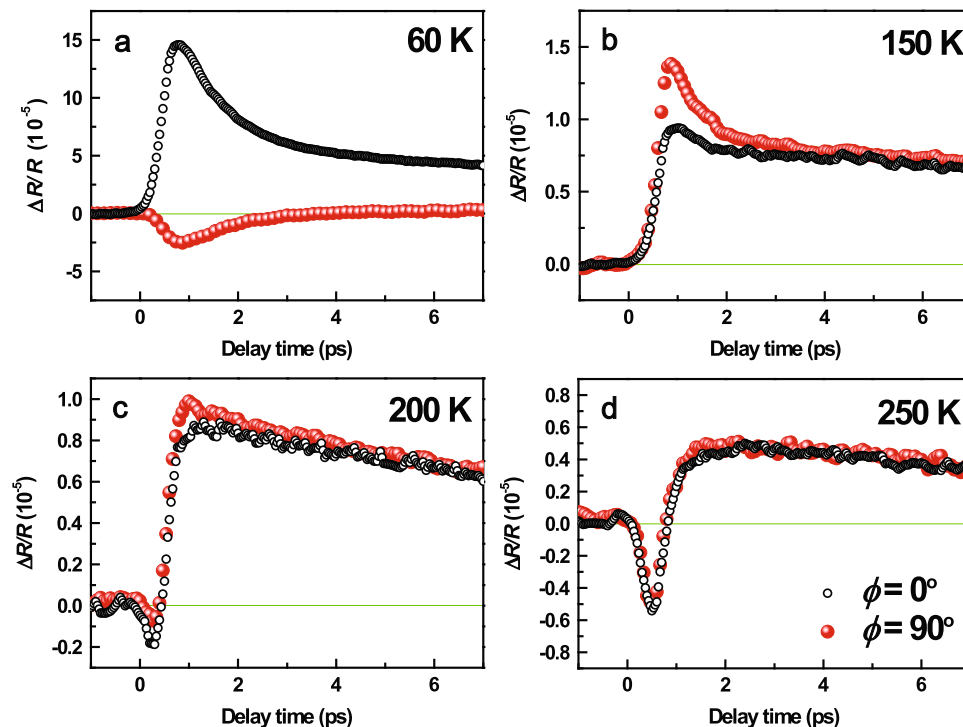


Fig. 2 a–d $\Delta R/R$ of an FeSe single crystal with the polarizations of pump and probe beams along $\phi = 0^\circ$ and 90° at various temperatures

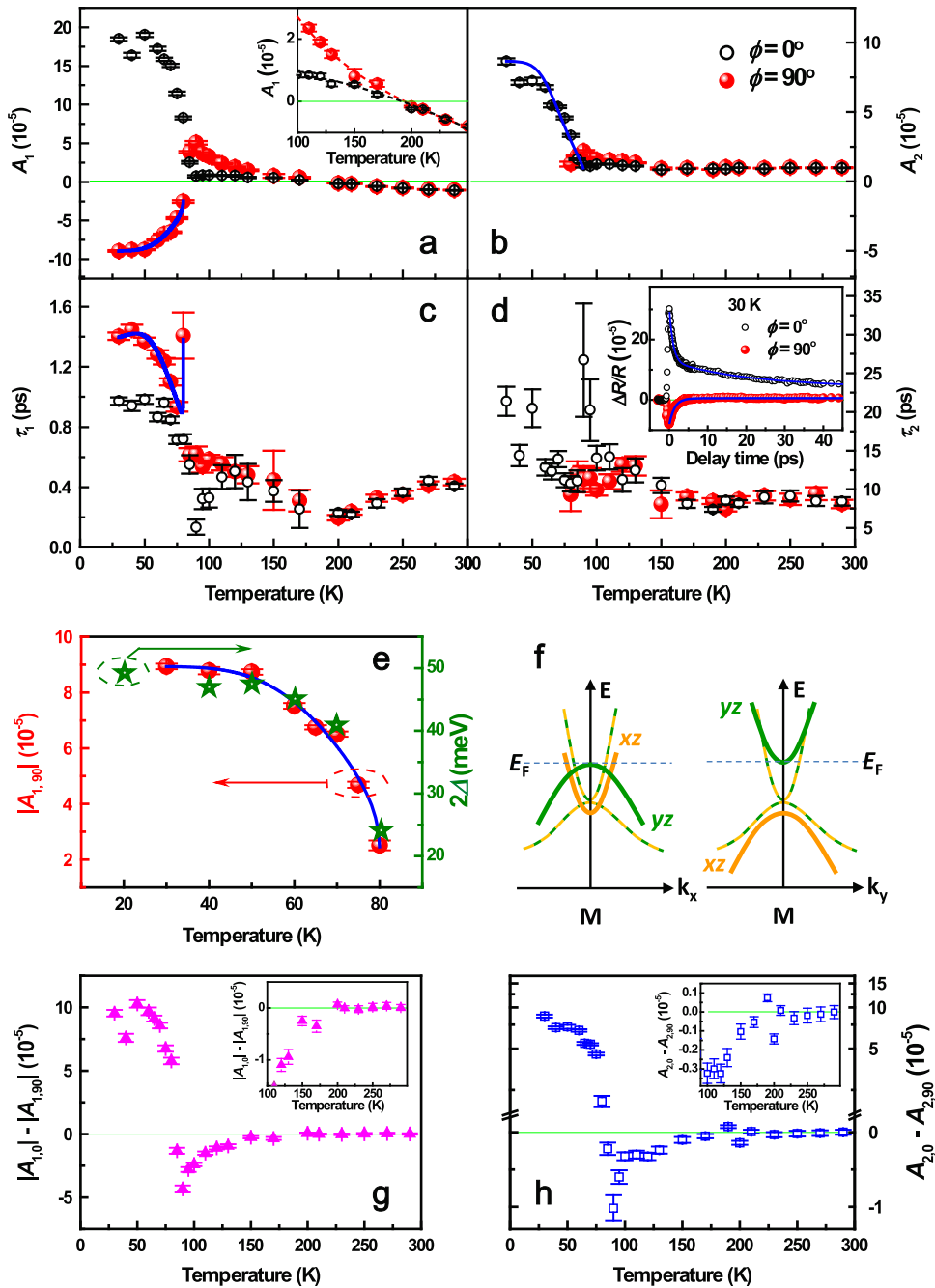


Fig. 3 Temperature dependence of the amplitudes **a** A_1 , **b** A_2 and the relaxation times **c** τ_1 , **d** τ_2 of $\Delta R/R$ along $\phi = 0^\circ$ and 90° resulting from the fits by Eq. 1. Solid lines are fits to the Rothwarf–Taylor model in **a–c** (see sections S3 and S4 in Supplementary Information). Inset of **a** shows the temperature-dependent A_1 on an enlarged scale. Inset of **d** shows the $\Delta R/R$ along $\phi = 0^\circ$ and 90° at 30 K as an example, fit by Eq. 1. **e** Amplitude A_1 of **a** below T_s fitted with the Rothwarf–Taylor model (solid line). The solid stars show the temperature-dependent band splitting along k_y at M point obtained by ARPES.²⁷ **f** The band structure along k_x and k_y at M point for $T < T_s$ (thick-solid lines) and $T > T_s$ (thin-dashed lines).²⁷ **g** Difference between $A_{1,0}$ ($\phi = 0^\circ$) and $A_{1,90}$ ($\phi = 90^\circ$) in **a**. Inset shows the temperature range above T_s . **h** The difference between $A_{2,0}$ ($\phi = 0^\circ$) and $A_{2,90}$ ($\phi = 90^\circ$) in **b**. Inset shows the enlarged part above T_s . The error bars are the standard deviations estimated from several measurements

$A_{1,0}$ below T_s is positive; in contrast, that of $A_{1,90}$ below T_s is negative for $\phi = 90^\circ$. In the literature, this difference is known to manifest the nematicity of the electronic structure. For example, the anisotropic single-particle and collective excitations in the quasi-1D charge-density wave semiconductor $\text{K}_{0.3}\text{MoO}_3$ ³⁷ and the d -wave symmetry of the superconducting gap in cuprate superconductors YBCO^{38–41} have been unambiguously revealed by polarized pump–probe spectroscopy. As intriguingly, the orientation anisotropy is shown also in τ_1 (Fig. 3c). $\tau_{1,90}$ for $\phi = 90^\circ$

(red solid circles) shows a notable divergence near T_s ; this divergence in the rate of QP relaxation indicates a gap opening, at least on some part of the FS. The presence of a gap in the QP density of states gives rise to a bottleneck for carrier relaxation. The mechanism of the bottleneck is described by the Rothwarf–Taylor model;⁴² indeed, the temperature dependence of $\tau_{1,90}$ was perfectly fitted according to that model as denoted by the blue solid line in Fig. 3c. Within the same context, $A_{1,90}$ was also fitted, as shown by the blue solid line in Fig. 3e. Assuming a mean-

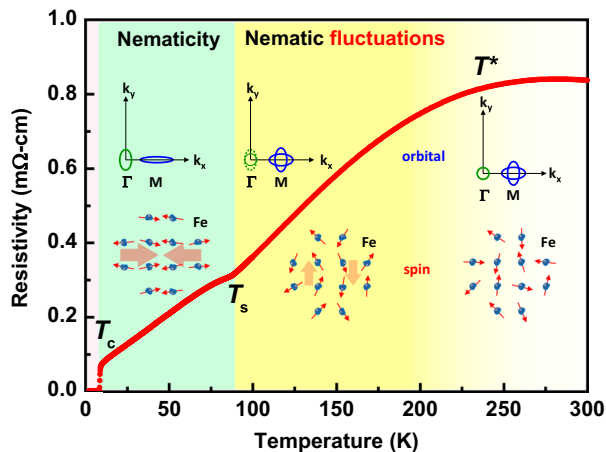


Fig. 4 Phase diagram of FeSe by nematic ultrafast dynamics. Temperature dependence of the resistivity ρ shows clearly an anomaly at T_s and indicates the high quality of FeSe together with a large residual-resistance ratio (RRR). T^* denotes the temperature at which $\rho(T)$ shows a rapid change of slope. *Insets* illustrate the nematic evolution of charge and spin subsystems in various phases. The *thin arrows* indicate sketchily the individual moment of Fe ions. The *thick arrows* indicate the “net” magnetic moments of FeSe in the stripe form. The simplified FS in each temperature range is depicted. The picture of FS for $T < T_s$ follows ref. 49. The *dashed green line* denoted the proposed FS fluctuations at the Γ point

field-like temperature-dependent $\Delta(T) = \Delta(0) [1 - (T/T_s)]^x$, the fit of $A_{1,90}$ leads to a gap amplitude $2\Delta(0) = 8.14k_B T_s = 56$ meV, consistent with the energy splitting between d_{yz} and d_{xz} near the M point in the Brillouin zone revealed from ARPES;^{27, 28} details of the fitting and discussions are available in section S3 of Supplementary Information. Furthermore, the temperature dependence of $\Delta(T)$ is totally consistent with that of the splitting energy at the M point as shown by the *solid stars* in Fig. 3e. However, there is no such signature of divergence for $\tau_{1,0}$ near T_s , which implies a major difference in carrier dynamics and in the band structure along various \mathbf{k} orientations in the electronic structure. This discrepancy between $\tau_{1,0}$ and $\tau_{1,90}$ seems puzzling, but it actually fits well into the fascinating ARPES observation that, for $T < T_s$ at M point, a gap is opened along k_y , whereas there is no gap opening along k_x (see the illustration of the band structure in Fig. 3f).²⁷ It is therefore plausible to assign the directions of 0° and 90° as x and y , respectively. The abrupt decrease in $\tau_{1,0}$ at 90 K, i.e., the relaxation of QPs becoming efficient, probably indicates that an increased density of states is involved in the relaxation processes along k_x .^{43, 44} In this scenario, the results of Fig. 3a, c also imply that the reconstruction of FS at the M point occurs mainly near 90 K, with no significant fluctuation of electronic nematicity at the M point above 100 K. As ultrafast spectroscopy is a bulk probe, the present results provide bulk evidence to support the electronic structure according to the surface-sensitive ARPES.

We turn to the slow component in Eq. 1 associated with A_2 and τ_2 below T_s . The high-energy QPs accumulate in the d conduction band of Fe and release their energy through the emission of longitudinal-optical (LO) phonons within a couple of picoseconds. The QPs (or LO phonons) would subsequently also transfer their energy to the spin subsystem and then disturb the spin ordering on the timescale of tens of picoseconds.⁴⁵ This spin-related mechanism was clearly observed in this work as represented by A_2 and τ_2 in Fig. 3b, d. As the temperature decreases, the stronger interaction between spins further results in an extended τ_2 to disturb the spin subsystem. The nematicity of the slow component is even more pronounced than that of the fast component. While $A_{2,0}$ can be clearly found below T_s and increases with decreasing T , there is no slow component of $\Delta R/R$ along $\phi = 90^\circ$ (as shown by both the data

and the fits in the inset of Fig. 3d). This fact implies that, although there is no magnetic order observed in FeSe down to the lowest temperatures, there does exist a strongly anisotropic spin subsystem with the energy scale of ~ 72 meV (details are available in section S4 of Supplementary Information) below T_s , which is consistent with the value obtained from inelastic neutron scattering.⁴⁶ In general, the responsive spin orientation is parallel to the polarization of the pump and probe beams. Most spins hence tend to align along direction $x(a)$ as in most pnictides (see, e.g. refs. 47–49), albeit with a short-range order. This mechanism opens an additional relaxation channel for QP decay along $\phi = 0^\circ$. About at T_s , the divergence in τ_2 implies the setting of the nematic coupling to the spin subsystem (Fig. 3d), which is caused by the sudden alignment of spins along x (ref. 8) in the nematic phase.^{9, 17, 20} Very recently, NMR experiments have observed the strong low-energy magnetic fluctuations below T_s ,⁴⁷ neutron-scattering experiments have identified the $(\pi, 0)$ fluctuation wave vector.^{8, 9} The origin of magnetism below T_s in FeSe is likely associated with an imbalance of the occupied electron numbers $n_{xz} > n_{yz}$, which is mainly due to the band splitting at the M point below T_s .⁵⁰ Within this context, there exists a coupling between the direction of spins and the orientation of the FS distortion through the nematicity of $n_{xz} - n_{yz}$. The direction of spins would likely follow the elongation direction of FS, as in the case of pnictides.⁴⁹ Overall, the results from the present work on the nematic ultrafast dynamics are illustrated in the green-colored nematic order phase of Fig. 4.

DISCUSSION

The state of $T > T_s$ in FeSe has been much less revealed than in the nematic phase, partly due to the lack of tools appropriate to investigate the nematic fluctuations. In the following, we show that nematic ultrafast dynamics above T_s elucidates surprising details of this largely uncharted territory. As shown in Figs. 1–3, when T increases beyond T_s , the nematic signatures persist until at least 200 K. In comparison, the magnitude of $\Delta R/R$ for $T > T_s$ is smaller than that for $T < T_s$, but two features of the fast component directly appear. (i) The polarity of A_1 reverses sign immediately for $T > T_s$, as seen in Fig. 3a and more clearly with $|A_{1,0}| - |A_{1,90}|$ in Fig. 3g. (ii) With decreasing T , the nematic signature in A_1 emerges at 200 K, shown in the inset of Fig. 3a. At low temperatures below T_s , the FS elongation at the Γ point was reported to be with an orientation by 90° relative to the FS elongation direction at the M point (Fig. 4).²² Enlightened by this drastic FS reconstruction, we propose a scenario of the state in FeSe for $T > T_s$ to reconcile both features (i) and (ii). In the high-temperature tetragonal phase, FS of FeSe has C_4 symmetry. When temperature is decreased to ~ 200 K, with the FS at the M point retaining C_4 symmetry, the nematic fluctuations at the Γ point emerges. As FS reconstruction or any fluctuation at the M point is still absent in this temperature range, the QP relaxation changes probed above T_s are dominated by the FS fluctuations at the Γ point. The consequent nematic sign of $|A_{1,0}| - |A_{1,90}|$ between 90 and 200 K is opposite to that below T_s , since the orientations of FS elongation at the M and Γ points are just opposite below T_s . This scenario is shown schematically in Fig. 4. It is noted that at $T < T_s$ the electronic nematicity is dominated by the FS reconstruction at the M point, for the FS reconstruction at the Γ point is less severe than at the M point.^{10, 14–16, 26–28} It is also worth noting that, with almost equal $\tau_{1,0}$ and $\tau_{1,90}$ above T_s shown in Fig. 3c, the QP relaxation dynamics along k_x and k_y are almost the same with nematic fluctuations at the Γ point. This effect is in contrast to the case of anisotropic τ below T_s , which is dominated by the FS reconstruction at the M point.

The slow component with spin coupling further unveils previously elusive magnetic properties of the regime for $T > T_s$. At high temperatures, $A_{2,0} - A_{2,90} = 0$ as seen clearly in Fig. 3h. The lack of nematic fluctuations in the slow component indicates

that the average magnetic moments along x and y directions are the same, reflecting the continuous rotational symmetry. Nevertheless, with decreasing T , the nematic signal of $A_{2,0} - A_{2,90} \neq 0$ clearly shows at about $T = 150$ K (see Fig. 3h and the *inset*). This nematic signal of A_2 indicates the onset of a magnetic subsystem breaking the four-fold symmetry. Very recently, the existence of magnetic fluctuations at $T = 110$ K has been reported by inelastic neutron scattering.⁴⁶ However, the existence of magnetic fluctuations between T_s and up to at least 150 K has not been discovered until in the present work. Moreover, the sign of $A_{2,0} - A_{2,90} < 0$ is opposite to that below T_s , indicating that the fluctuating spins tend to align along the y direction. This rotation of the spin direction by 90° above T_s is coupled to the fluctuating FS elongation at the Γ point with an orientation by 90° relative to that at the M point below T_s . (An alternative origin of these differences is the sign inversion of the orbital polarization at the Γ point unique to FeSe, which produces $n_{xz} > n_{yz}$, in contrast to the FS reconstruction at the M point below T_s . The orbital polarization at the Γ point is related to the band splitting that exists above T_s and was observed by ARPES.²⁸ The origin of the band splitting at the Γ point remains elusive,²⁸ but is unlikely due to nematic fluctuations for $T > T_s$ since regular ARPES probes static orders.) Overall, we have observed both nematic and magnetic fluctuations in FeSe at high temperatures. The coupling between the magnetic fluctuations and the change of the electronic structure at high temperatures are also identified, as below T_s . The regime with the newly discovered nematic and magnetic fluctuations is denoted by the yellow area in Fig. 4. Careful measurements of the magnetic properties support an onset of the magnetic fluctuations at a temperature far above T_s , as shown in section S5 of Supplementary Information. The distinct FS elongation directions at the M and Γ points weaken the FS nesting. This effect is likely a key to the absence of static magnetic order in FeSe. There are more discussions in section S5 of Supplementary Information on the temperature range of the nematic and magnetic fluctuations above T_s . The onset temperature of the magnetic fluctuations is, notably, near T^* , at which the slope of $\rho(T)$ demonstrates a rapid change (Fig. 4). These results hint at a nematic/magnetic origin of T^* .

Finally, the nematic ultrafast QP dynamics in FeSe has been thoroughly studied by polarized pump-probe spectroscopy. Two distinct relaxation components were observed in $\Delta R/R$. The fast component on the time scale 0.1–1.5 ps associated with the electronic structure and the slow component on the time scale 8–25 ps assigned to the energy relaxation through the spin channel together elucidate an exotic phase diagram of FeSe shown in Fig. 4, where both nematic fluctuations and an elusive spin subsystem are hidden above T_s . The present results certainly inspire a possible scenario for all Fe-based superconductors, which needs to be confirmed by other probes.

METHODS

We grew FeSe single crystals in evacuated quartz with a KCl–AlCl₃ flux technique.⁵¹ The crystalline structure and transport properties of the samples were examined by X-ray diffraction and van der Pauw measurements, respectively. The femtosecond spectroscopy measurement was performed with a dual-color pump-probe system (for the femtosecond laser, the repetition rate 5.2 MHz, wavelength 800 nm, pulse duration 100 fs) and an avalanche photodetector with the standard lock-in technique. This non-degenerate pump-probe scheme can significantly eliminate the annoying coherent spike around zero time delay.⁵² The fluences of the pump and probe beams were 39.7 and 2.3 $\mu\text{J}/\text{cm}^2$, respectively. The pump pulses have a corresponding photon energy of 3.1 eV at which greater absorption occurred in the absorption spectrum of FeSe,⁵³ and hence generate electronic excitation. To study the QP dynamics, we measured the photoinduced reflectivity ($\Delta R/R$) transients of the probe beam with photon energy 1.55 eV. $\Delta R/R(t, \phi_{\text{pump, probe}})$ curves along various orientations on the surface of the sample were obtained on

rotating the polarization of pulses at nearly normal incidence ($\theta_{\text{pump}} \sim 0^\circ$, $\theta_{\text{probe}} \sim 7^\circ$). The intensity and polarization (electric field, \mathbf{E}) of pulses were adjusted with a $\lambda/2$ plate and polarizer.^{38–41} Moreover, the penetration depth of FeSe is ~ 24 nm for 400 nm and ~ 30 nm for 800 nm, which are estimated from the skin depth of electromagnetic wave in metal, $\lambda/4\pi k$.¹¹

The spot size of the probe beam in this study is $83 \times 45 \mu\text{m}$, which is smaller than the typical domain size of $\sim 400 \times 200 \mu\text{m}$ in our FeSe single crystals, as shown in Fig. S1 of Supplementary Information. Due to the external stress, e.g., caused by the glue/holder, each domain has its own preferred orientation once the nematicity and even nematic fluctuations appear. In addition, while the general static measurement (e.g., ARPES) is a probe into the static orders of FeSe, the transient pump-probe spectroscopy is capable of probing the orders that fluctuate fast or the short-range order. This is because, after the fluctuation order is destroyed by a pumping pulse, we can immediately probe the reforming fluctuation order within femtosecond timescale. However, the general static measurements do not provide enough time-resolution to resolve these fast fluctuations and only can obtain the long-time average results, which is usually zero. Moreover, there is no trigger signal (served by a pump pulse) to be a reference point in time domain for the general static measurements.

Data availability

The authors declare that the data supporting the findings of this study are available within the paper and its [Supplementary Information](#) files.

ACKNOWLEDGEMENTS

This work is supported by the Ministry of Science and Technology of the Republic of China, Taiwan (Grant No. 102-2112-M-009-006-MY3, 103-2923-M-009-001-MY3, 103-2628-M-00-002-MY3, 103-2119-M-009-004-MY3, 103-2119-M-009-007-MY3, and 103-2112-M009-015-MY3) and the Grant MOE ATU Program at NCTU. This work was also supported by the Ministry of Education and Science of the Russian Federation in the framework of Increase Competitiveness Program of NUST “MISIS” No. K2-2016-066 and by Act 211 Government of the Russian Federation, contracts No. 02.A03.21.0006 and 02.A03.21.0011. We gratefully acknowledge P. H. Lin (NSRRC) for the discussion of ARPES and the assistance of C.-M. Cheng (NSRRC) for the manuscript.

AUTHOR CONTRIBUTIONS

C.W.L. developed the polarized pump-probe spectroscopy. P.C.C. and S.H.W. performed the pump-probe experiments and analyzed the data. J.C.C. carried out the $\chi(T)$ measurements of the samples. D.A.C., O.S.V., and A.N.V. synthesized and characterized the FeSe crystals. The manuscript was written by C.W.L. and J.Y.L. with the assistance from J.Y.J. and K.H.W. All authors discussed the results and commented the manuscript.

ADDITIONAL INFORMATION

Supplementary Information accompanies the paper on the *npj Quantum Materials* website (doi:[10.1038/s41535-017-0036-5](https://doi.org/10.1038/s41535-017-0036-5)).

Competing interests: The authors declare no competing financial interests.

Publisher's note: Springer Nature remains neutral with regard to jurisdictional claims in published maps and institutional affiliations.

REFERENCES

- Kamihara, Y., Watanabe, T., Hirano, M. & Hosono, H. Iron-based layered superconductor $\text{La}[\text{O}_{1-x}\text{F}_x]\text{FeAs}$ ($x=0.05\text{--}0.12$) with $T_c=26$ K. *J. Am. Chem. Soc.* **130**, 3296–3297 (2008).
- Johnston, D. C. The puzzle of high temperature superconductivity in layered iron pnictides and chalcogenides. *Adv. Phys.* **59**, 803–1061 (2010).
- Hirschfeld, P. J., Korshunov, M. M. & Mazin, I. I. Gap symmetry and structure of Fe-based superconductors. *Rep. Prog. Phys.* **74**, 124508 (2011).
- Chu, J. H. et al. R. In-plane resistivity anisotropy in an underdoped iron arsenide superconductor. *Science* **329**, 824–826 (2010).
- Chu, J. H., Kuo, H. H., Analytis, J. G. & Fisher, I. R. Divergent nematic susceptibility in an iron arsenide superconductor. *Science* **337**, 710–712 (2012).
- Fernandes, R. M., Chubukov, A. V. & Schmalian, J. What drives nematic order in iron-based superconductors? *Nat. Phys.* **10**, 97–104 (2014).

7. Hsu, F. C. et al. Superconductivity in the PbO-type structure α -FeSe. *Proc. Natl Acad. Sci. USA* **105**, 14262–14264 (2008).
8. Rahn, M. C., Ewings, R. A., Sedlmaier, S. J., Clarke, S. J. & Boothroyd, A. T. Strong $(\pi, 0)$ spin fluctuations in β -FeSe observed by neutron spectroscopy. *Phys. Rev. B* **91**, 180501(R) (2015).
9. Wang, Q. et al. Strong interplay between stripe spin fluctuations, nematicity and superconductivity in FeSe. *Nat. Mater.* **15**, 159–163 (2016).
10. Zhang, Y. et al. Distinctive momentum dependence of the band reconstruction in the nematic state of FeSe thin film. Preprint at <http://arXiv.org/abs/1503.01556> (2015).
11. Luo, C. W. et al. Quasiparticle dynamics and phonon softening in FeSe superconductors. *Phys. Rev. Lett.* **108**, 257006 (2012).
12. Xu, H. C. et al. Direct observation of the bandwidth control Mott transition in the $\text{NiS}_{2-x}\text{Se}_x$ multiband system. *Phys. Rev. Lett.* **112**, 087603 (2014).
13. Terashima, T. et al. Anomalous Fermi surface in FeSe seen by Shubnikov–de Haas oscillation measurements. *Phys. Rev. B* **90**, 144517 (2014).
14. Nakayama, K. et al. Reconstruction of band structure induced by electronic nematicity in an FeSe superconductor. *Phys. Rev. Lett.* **113**, 237001 (2014).
15. Watson, M. D. et al. Emergence of the nematic electronic state in FeSe. *Phys. Rev. B* **91**, 155106 (2015).
16. Chubukov, A. V., Fernandes, R. M. & Schmalian, J. Origin of nematic order in FeSe. *Phys. Rev. B* **91**, 201105 (2015).
17. Glasbrenner, J. K. et al. Effect of magnetic frustration on nematicity and superconductivity in iron chalcogenides. *Nat. Phys.* **11**, 953–958 (2015).
18. Mukherjee, S., Kreisel, A., Hirschfeld, P. J. & Andersen, B. M. Model of electronic structure and superconductivity in orbitally ordered FeSe. *Phys. Rev. Lett.* **115**, 026402 (2015).
19. Watson, M. D. et al. Dichotomy between the hole and electron behavior in the multiband FeSe probed by ultrahigh magnetic fields. *Phys. Rev. Lett.* **115**, 027006 (2015).
20. Wang, F., Kivelson, S. A. & Lee, D.-H. Nematicity and quantum paramagnetism in FeSe. *Nat. Phys.* **11**, 959–963 (2015).
21. Luo, C. W. et al. Ultrafast dynamics and phonon softening in $\text{Fe}_{1+y}\text{Se}_{1-x}\text{Te}_x$ single crystals. *New J. Phys.* **14**, 103053 (2012).
22. Song, C.-L. et al. Direct observation of nodes and twofold symmetry in FeSe superconductor. *Science* **332**, 1410–1413 (2011).
23. Abdel-Hafiez, M. et al. Temperature dependence of lower critical field $H_{c1}(T)$ shows nodeless superconductivity in FeSe. *Phys. Rev. B* **88**, 174512 (2013).
24. Moore, S. A. et al. Evolution of the superconducting properties in $\text{FeSe}_{1-x}\text{S}_x$. *Phys. Rev. B* **92**, 235113 (2015).
25. Schütt, M., Schmalian, J. & Fernandes, R. M. Origin of DC and AC conductivity anisotropy in iron-based superconductors: scattering rate versus spectral weight effects. *Phys. Rev. B* **94**, 075111 (2016).
26. Maletz, J. et al. Unusual band renormalization in the simplest iron-based superconductor FeSe_{1-x} . *Phys. Rev. B* **89**, 220506(R) (2014).
27. Shimojima, T. et al. Lifting of xz/yz orbital degeneracy at the structural transition in detwinned FeSe. *Phys. Rev. B* **90**, 121111(R) (2014).
28. Zhang, P. et al. Observation of two distinct d_{xz}/d_{yz} band splittings in FeSe. *Phys. Rev. B* **91**, 214503 (2015).
29. Fedorov, A. et al. Effect of nematic ordering on electronic structure of FeSe. *Sci. Rep.* **6**, 36834 (2016).
30. Watson, M. D. et al. Evidence for unidirectional nematic bond ordering in FeSe. *Phys. Rev. B* **94**, 201107(R) (2016).
31. Lin, J.-Y. et al. Coexistence of isotropic and extended s -wave order parameters in FeSe as revealed by low-temperature specific heat. *Phys. Rev. B* **84**, 220507(R) (2011).
32. Zeng, B. et al. Anisotropic structure of the order parameter in $\text{FeSe}_{0.45}\text{Te}_{0.55}$ revealed by angle-resolved specific heat. *Nat. Commun.* **1**, 112 (2010).
33. Shih, H. C. et al. Magnetization dynamics and the Mn^{+3} d - d excitation of hexagonal HoMnO_3 single crystals using wavelength-tunable time-resolved femtosecond spectroscopy. *Phys. Rev. B* **80**, 024427 (2009).
34. Stojchevska, L., Mertelj, T., Chu, J., Fisher, I. R. & Mihailovic, D. Doping dependence of femtosecond quasiparticle relaxation dynamics in $\text{Ba}_{0.6}\text{K}_{0.4}\text{Fe}_2\text{As}_2$ single crystals: evidence for normal-state nematic fluctuations. *Phys. Rev. B* **86**, 024519 (2012).
35. Mertelj, T., Stojchevska, L., Zhigadlo, N. D., Karpinski, J. & Mihailovic, D. Normal state bottleneck and nematic fluctuations from femtosecond quasiparticle relaxation dynamics in $\text{Sm}(\text{Fe}, \text{Co})\text{AsO}$. *Phys. Rev. B* **87**, 174525 (2013).
36. Thewalt, E. et al. Optical evidence of broken C_4 symmetry across optimal doping in $\text{BaFe}_2(\text{As}_{1-x}\text{P}_x)_2$. Preprint at <http://arXiv.org/abs/1507.03981v2> (2015).
37. Demsar, J., Biljaković, K. & Mihailovic, D. Single particle and collective excitations in the one-dimensional charge density wave solid $\text{K}_{0.3}\text{MoO}_3$ probed in real time by femtosecond spectroscopy. *Phys. Rev. Lett.* **83**, 800 (1999).
38. Luo, C. W. et al. Dichotomy of photoinduced quasiparticle on CuO_2 planes of $\text{YBa}_2\text{Cu}_3\text{O}_{7-x}$ directly revealed by femtosecond polarization spectroscopy. *J. Appl. Phys.* **102**, 033909 (2007).
39. Luo, C. W. et al. Spatial symmetry of the superconducting gap of $\text{YBa}_2\text{Cu}_3\text{O}_{7-\delta}$ obtained from femtosecond spectroscopy. *Phys. Rev. B* **68**, 220508(R) (2003).
40. Luo, C. W. et al. Spatially resolved relaxation dynamics of photoinduced quasiparticles in underdoped $\text{YBa}_2\text{Cu}_3\text{O}_{7-\delta}$. *Phys. Rev. B* **72**, 092506 (2005).
41. Luo, C. W. et al. Spatial dichotomy of quasiparticle dynamics in underdoped thin-film $\text{YBa}_2\text{Cu}_3\text{O}_{7-\delta}$ superconductors. *Phys. Rev. B* **74**, 184525 (2006).
42. Rothwarf, A. & Taylor, B. N. Measurement of recombination lifetimes in superconductors. *Phys. Rev. Lett.* **19**, 27–30 (1967).
43. Sánchez-Barriga, J. et al. Ultrafast spin-polarization control of Dirac fermions in topological insulators. *Phys. Rev. B* **93**, 155426 (2016).
44. Luo, C. W. et al. Snapshots of Dirac fermions near the Dirac point in topological insulators. *Nano Lett.* **13**, 5797–5802 (2013).
45. Ogasawara, T. et al. General features of photoinduced spin dynamics in ferromagnetic and ferrimagnetic compounds. *Phys. Rev. Lett.* **94**, 087202 (2005).
46. Wang, Q. et al. Magnetic ground state of FeSe. *Nat. Commun.* **7**, 12182 (2016).
47. Baek, S.-H. et al. Orbital-driven nematicity in FeSe. *Nat. Mater.* **14**, 210–214 (2015).
48. Xiao, Y. et al. Magnetic structure of EuFe_2As_2 determined by single-crystal neutron diffraction. *Phys. Rev. B* **80**, 174424 (2009).
49. Zhang, Y. et al. Symmetry breaking via orbital-dependent reconstruction of electronic structure in detwinned NaFeAs . *Phys. Rev. B* **85**, 085121 (2012).
50. Suzuki, Y. et al. Momentum-dependent sign inversion of orbital order in superconducting FeSe. *Phys. Rev. B* **92**, 205117 (2015).
51. Chareev, D. et al. Single crystal growth and characterization of tetragonal FeSe_{1-x} superconductors. *Cryst. Eng. Commun.* **15**, 1989–1993 (2013).
52. Luo, C. W., Wang, Y. T., Chen, F. W., Shih, H. C. & Kobayashi, T. Eliminate coherence spike in reflection-type pump-probe measurements. *Opt. Express* **17**, 11321–11327 (2009).
53. Wu, X. J. et al. On the nature of the carriers in ferromagnetic FeSe. *Appl. Phys. Lett.* **90**, 112105 (2007).



Open Access This article is licensed under a Creative Commons Attribution 4.0 International License, which permits use, sharing, adaptation, distribution and reproduction in any medium or format, as long as you give appropriate credit to the original author(s) and the source, provide a link to the Creative Commons license, and indicate if changes were made. The images or other third party material in this article are included in the article's Creative Commons license, unless indicated otherwise in a credit line to the material. If material is not included in the article's Creative Commons license and your intended use is not permitted by statutory regulation or exceeds the permitted use, you will need to obtain permission directly from the copyright holder. To view a copy of this license, visit <http://creativecommons.org/licenses/by/4.0/>.

© The Author(s) 2017